Earth, Planets and Space

TECHNICAL REPORT

Open Access

Development of a laboratory monitoring system for elastic waves transmitted through sand under dry and nearly saturated conditions

Masayuki Nakayama[1*], Hironori Kawakata[2], Shiro Hirano[2] and Issei Doi[3]

Abstract

Laboratory experiments with seismic measurements have the potential to be highly useful for understanding the physical process of water-induced landslides, and fundamental experiments are helpful for the appropriate interpretation of recorded seismograms. We developed a laboratory measurement system to investigate the relationships between wave propagation and water saturation in sand. We considered that the wavelength should be comparable to or sufficiently shorter than the sensing intervals. Furthermore, we embedded a wave source that can repeatedly emit an arbitrary and identical signal in an octave frequency band under both dry and nearly saturated conditions. We measured the transmitted waves by embedded accelerometers over 24 h under dry and nearly saturated conditions. The difference in the slowness between the two conditions was one-thousand-fold larger than the fluctuations in slowness over 24 h for each condition. Also, the difference in amplitude between the two conditions was about double the fluctuations in amplitude over 24 h for each condition. These results suggested that our system can monitor the water content change in sand via the change in spectral amplitude and phase slowness.

Keywords: Wave propagation, Sand, Fluid saturation, Geohazard, Laboratory experiments, Porous materials

Introduction

Water-induced landslides caused by heavy rain or snowmelt are a significant geohazard and can cause severe damage to human society (e.g., Brückl et al. 2013; Wang et al. 2015; Zhou et al. 2015; García-Delgado et al. 2019). Water-induced landslides occur when rainwater or snowmelt infiltrates a potential failure plane and excessive pore water pressure occurs, which reduces the effective normal stress and in turn diminishes the available shear strength, thus resulting in slope failure (e.g., Zhou et al. 2015; Chen et al. 2018a, b; García-Delgado et al. 2019). The changes in physical properties of slopes due to water cause not only the decrease in the available shear strength, but also change in elastic wave velocity. Mainsant et al. (2012) measured seismic ambient noises across a slope by installing two receivers. They observed that the elastic wave velocity decreased gradually, followed by a sharp decrease occurring before the initiation of a major landslide. Laboratory experiments have been also performed to investigate the responses of elastic waves during slope failures. Chen et al. (2018a, b, 2019) developed an experimental slope sand model and measured transmitted waves through the model until a failure occurred. They observed a decrease in velocity before the main failure that followed the same trend as the field observation by Mainsant et al. (2012). This suggests that laboratory experiments have a high potential for contributing to the understanding of the physical process of landslides. However, the recorded elastic waves indicated the slope responses when many elemental processes interacted in

*Correspondence: res.nkym@gmail.com
[1] Graduate School of Science and Engineering, Ritsumeikan University, 1-1-1, Noji-Higashi, Kusatsu, Shiga 525-8577, Japan
Full list of author information is available at the end of the article

a complex fashion that may affect the elastic properties of the slopes, which makes it difficult to discern how each process affects the elastic wave velocity. To utilize this potential, more fundamental experiments should be performed to investigate the responses of the waves in individual elemental processes.

One of the most elemental processes is change in the degree of water saturation in a quasi-static process. Some previous studies transmitted waves around a specific frequency by giving a pulsive force and monitored the waves through sand under various degree of water saturation (Emerson and Foray 2006; George et al. 2009; Barrière et al. 2012; Lorenzo et al. 2013; Taylor et al. 2019). However, three concerns remain after these studies: (a) their analyses were performed around a specific frequency (all these studies), (b) the coupling between the source and the sand may change when a larger amplitude source causes larger inelastic strain in the vicinity of the source in wet sand (all these studies), and (c) the impact-induced source (Emerson and Foray 2006; Barrière et al. 2012) may have difficulty in emitting arbitrary and highly reproducible signals.

For the first concern (a), we considered the required conditions for elastic waves in field monitoring. We adopted two parameters: the wavelength λ and sensor intervals x. The parameter space is shown in Fig. 1. The interval x should be comparable to or one-tenth of the size of slope failures. The wavelength λ should be sufficiently shorter than x and the failure size and be broader to monitor failures in various sizes. However, λ in each previous experimental study was around a specific value. Although it is impossible to immediately compare laboratory experimental results and field observations because seismic wave attributes (velocity dispersion and attenuation) due to wave-induced fluid flow mechanism may differ in frequency ranges (ultrasonic, sonic and seismic) (Pride 2005), expanding the range of λ can help fill a gap in understanding the velocity dispersion and the attenuation in unconsolidated and porous media.

For the second concern (b), we considered the coupling between an elastic wave source and sand should be independent of dry/wet conditions. In some previous studies, elastic waves were radiated to sand via a granite plate (Barrière et al. 2012), a steel tube (Emerson and Foray 2006) or transducers (George et al. 2009; Taylor et al. 2019) all of which were attached on drying/wetting sand. Lorenzo et al. (2013) used transducers embedded in drying/wetting sand as an elastic wave source. In such ways, the coupling between an elastic wave source and sand may change more in wet sand as elastic waves with a larger amplitude are radiated. A technique should be applied which prevents any changes in the coupling between the source and sand due to change in the degree of water saturation.

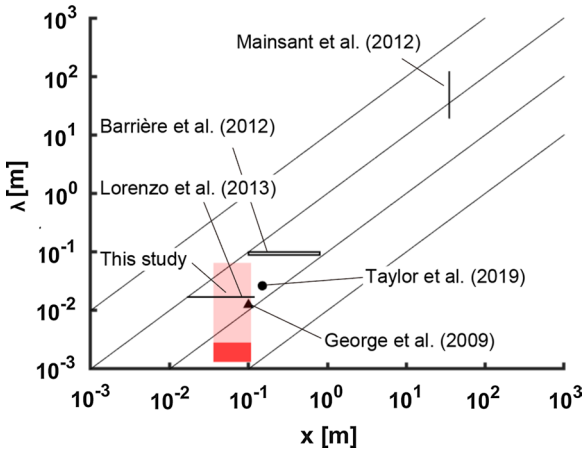

Fig. 1 Parameter space between wavelength λ and sensor intervals x. We used a velocity at a condition of dry or lower degree of water saturation or velocity profiles in situ (Mainsant et al. 2012) together with frequency of input signals or analyzed frequency, when we calculated λ. The velocities by George et al. (2009), Barrière et al. (2012), Mainsant et al. (2012), Lorenzo et al. (2013), Taylor et al. (2019), and this study were 250 m/s, 160 m/s, 475 m/s, 170 m/s, 264 m/s, and 65 m/s (refer to "Monitoring capability for water content change in our system" section), respectively. The light red solid rectangle represents our experimental conditions, and the red solid rectangle represents the range that we analyzed in detail

For the third concern (c), we considered power and reproducibility of emitted waves. As mentioned in (b), input signals with as small amplitude in a time series as possible should be applied not to disturb the vicinity of the source. Stacking technique is applicable to improve signal-to-noise (S/N) ratios in case of small source amplitude if source signal is reproducible. Emerson and Foray (2006) used a steel tube and a steel rod as an elastic wave source and Barrière et al. (2012) used a granite plate and a steel ball. Such simple techniques make it difficult to emit arbitrary and highly reproducible signals. We should use a source which can repeatedly emit arbitrary and identical waves with a small amplitude.

In this study, we developed a new wave monitoring system to investigate relationships between elastic wave propagation and water saturation in sand with a simplified experimental setup after addressing the above three concerns. We applied an internal elastic wave source that repeatedly emitted arbitrary and identical input signals with a broader frequency band (light red solid rectangle in Fig. 1). We measured the transmitted waves through the sand for 24 h under two static conditions, dry and nearly saturated, and estimated our system's capability of monitoring water content change.

Methodology

Experimental setup and procedures

We prepared sand in a container (375 mm L × 255 mm W × 235 mm H) as follows. The internal source's surroundings need to be protected from water infiltration. Thus, we separated the sand into a permeable part (PP) and an impermeable part (IP) and installed the source into the latter. We prepared PP so we could monitor transmitted waves under dry and nearly saturated conditions (Fig. 2). To prevent water infiltration into IP, we prepared a bentonite layer (BL) to enclose IP. Furthermore, IP was composed of water-repellent sand, so it remained dry even if some water passed through BL. BL except for the top surface was set up in the container in advance. BL had a thickness of 30 mm and was located 20 mm away from the source. Then, we dropped bare and water-repellent sand particles into PP and IP, respectively, from the top of the container. During the dropping process, instruments were placed at the designated position (see the following description) and buried. Finally, BL completely covered IP, and sand of about 100 mm thickness was produced. PP consisted of silica sand with particle diameters about 0.2–0.4 mm, and its dry density and porosity were 1.2×10^3 kg/m^3 and 54%, respectively.

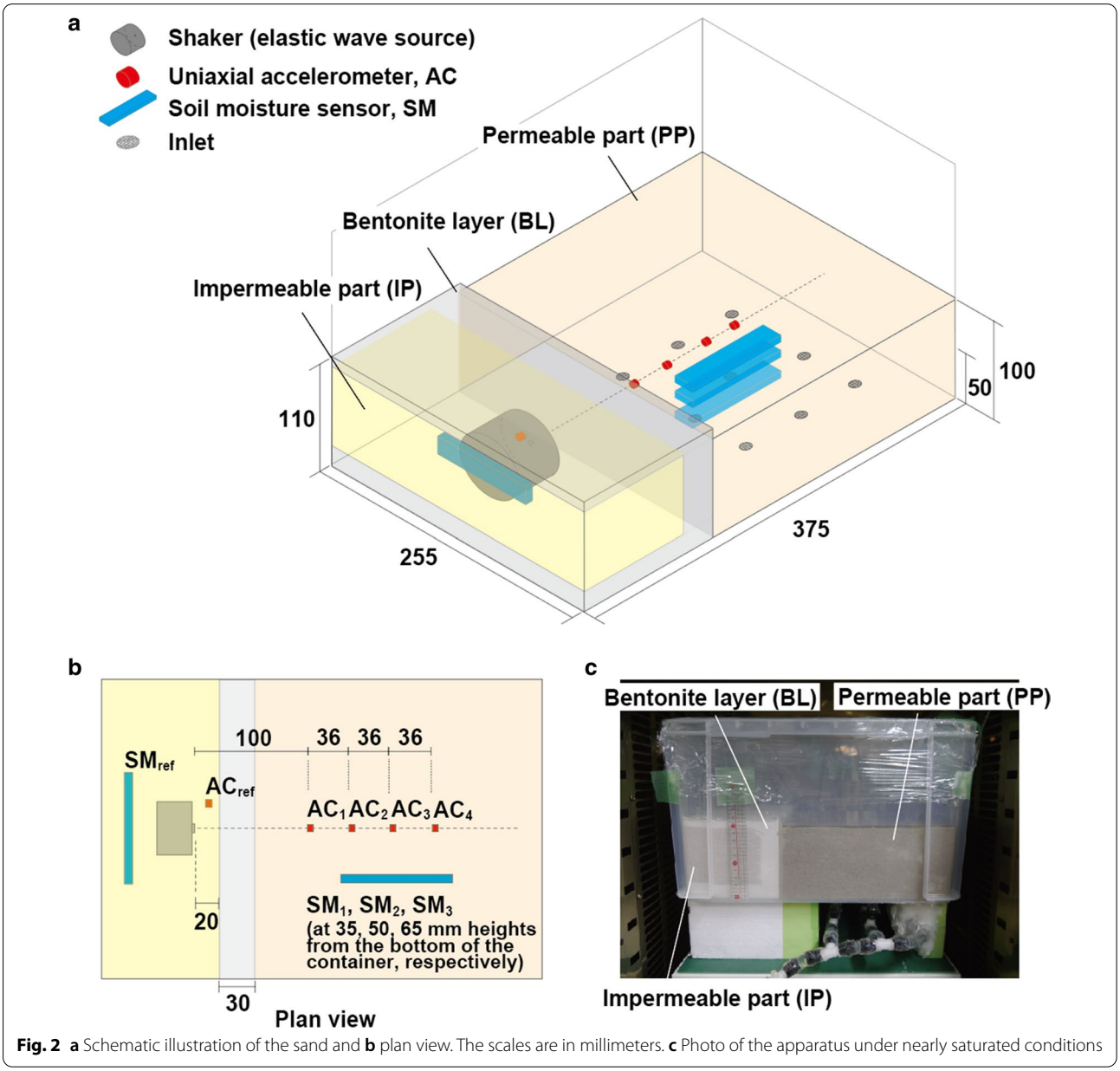

Fig. 2 **a** Schematic illustration of the sand and **b** plan view. The scales are in millimeters. **c** Photo of the apparatus under nearly saturated conditions

BL consisted of a mixture of sand and bentonite (2602 by Pepaless Co., Ltd.). IP consisted of sand sprayed with a water-repellent liquid (Dry Barrier 365 by Nano4life).

We used a general-purpose vibration speaker as an elastic wave source (referred to as a shaker). We installed it in IP at a 50 mm height from the bottom of the container so that its vibration was parallel to the long axis of the sand. Five uniaxial accelerometers (S04SG2 by Fuji Ceramics Corporation) were installed in the sand so that their faces were oriented toward the shaker (red solid cubes in Fig. 2). One of them, AC_{ref}, was installed a few centimeters away from the shaker to monitor the stability of the wave radiation. The others, AC_1, AC_2, AC_3, and AC_4, were installed into PP and aligned to be at the same height as the shaker. These accelerometers were spaced at 36 mm with hypocenter distances from 100 to 208 mm. The accelerometers were 3.5 mm in diameter and 2.5 mm thick, and the frequency response was within ± 7 dB below 50 kHz.

We needed to input a signal with enough spectral amplitude so that the transmitted waves had high S/N ratios at the far receivers. However, the signal power must be small enough to not irreversibly rearrange the sand particles in the vicinity of the source. Then, we adopted a linear sweep (chirp) signal, which can reduce the amplitude in a time series far below that of an impulsive or step-like signal by lengthening the oscillation time. In our experiments, a linear sweep signal that varied from 1 to 50 kHz and had a voltage of 5 Vpp and a duration of 0.5 s was repeatedly applied every 1.2 s to the shaker using a function generator FG (FG3102 by Tektronix, Inc.) and an amplifier (PS-3238 by EK JAPAN, Co., Ltd.). The output of the FG and the signals received by the accelerometers were simultaneously recorded through a 24-bit A/D converter (PXIe-4492 by National Instruments) at the sampling rate of 204.8 ksps.

Four moisture meters (EC-5 by METER Group, Inc.) were also installed in the sand to measure the volumetric water content in the sand (blue solid rectangular plates in Fig. 2). One of them, SM_{ref}, was installed near the shaker to check that the water did not infiltrate into IP. The others, SM_1, SM_2, and SM_3, were installed in PP at heights of 35 mm, 50 mm, and 65 mm from the bottom of the container, respectively. The data were recorded through a data logger (Em5b by METER Group, Inc.), and we obtained hourly averages of the volumetric water content data.

For the experimental procedures, first, the air-dried sand was placed in an oven (DH42 by Yamato Scientific Co., Ltd.) and dried at 40 °C for 24 h. Second, the transmitted waves were recorded for 24 h at the same temperature. Third, we slowly injected tap water (not degassed water) from inlets attached to the bottom of the container until the water level reached over the surface of PP. This procedure took about two hours. The sand was left as it was for 24 h at 40 °C so that the water flow during the injection calmed down. After that, the transmitted waves were recorded over 24 h at the constant temperature of 40 °C. We covered the sand with a vinyl sheet to prevent evaporation from the soil surface during undisturbed and monitoring periods. We confirmed that the water contents remained constant during the measurements of elastic waves, both in the dry and nearly saturated conditions, as determined from the records of the soil moisture meters.

Data processing procedures

First, we stacked the recorded waveforms as illustrated in Fig. 3. We extracted 1.2-s waveforms, including 0.5-s input signals, from the recorded waveforms at an interval of 1.2 s. We stacked the 1.2-s waveforms included in each 15-min window to improve the S/N ratios (Fig. 4). A fourth-order Butterworth band-pass filter from 0.1 to 100 kHz was applied to the stacked waveforms. Then, we extracted 0.6-s waveforms $u_i(t,\tau)$, including the 0.5-s sweep signals. Here, $i, t,$ and τ denote the channel labels (ref, 1, 2, 3, and 4), measurement time in hours ($0 \leq t \leq 24$ h), and time in seconds ($0 \leq \tau \leq 0.6$ s), respectively.

Second, we extracted only the response of the fundamental tone components of the stacked waveforms $u_i(t,\tau)$. Figure 4a shows a typical spectrogram of the stacked waveform for the input signal. We observed some overtones in addition to the fundamental tones, which were probably caused by the FG. Therefore, we extracted the spectra of the stacked waveforms $U_i(t,f)$ only for the fundamental tone components using the following:

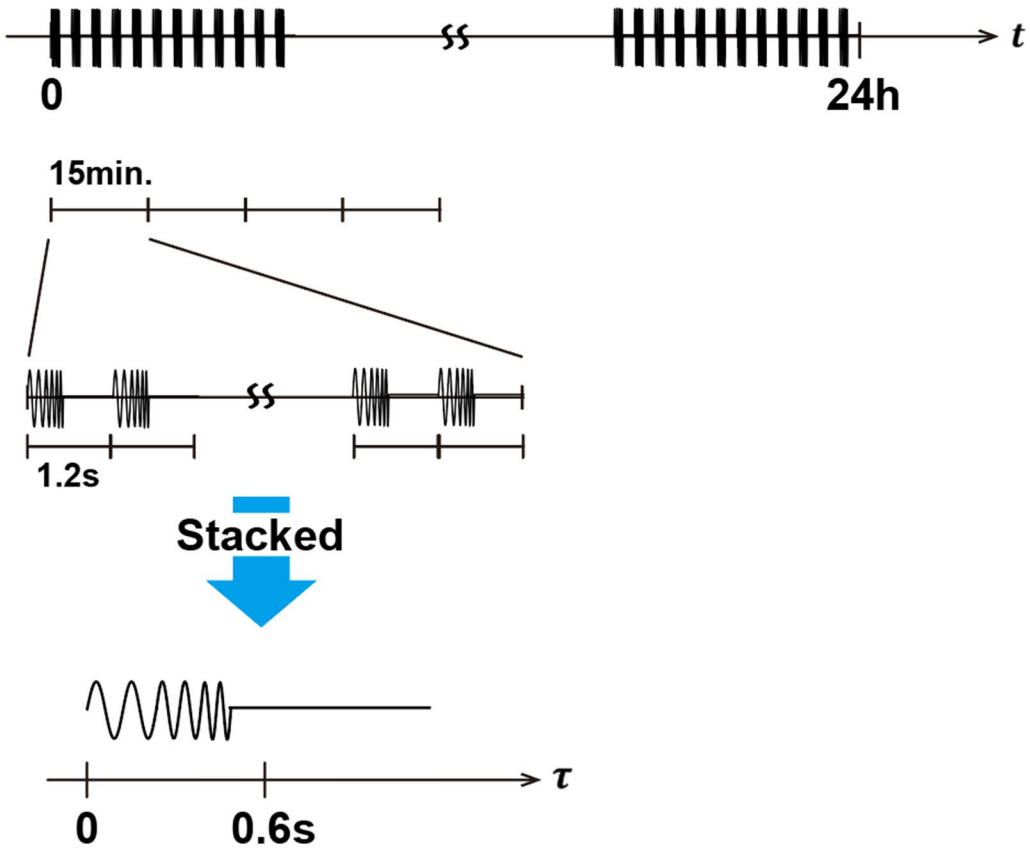

Fig. 3 Schematic illustration of wave stacking in our analysis

$$\begin{cases} U_i(t,f) = \displaystyle\int_0^{0.6} u_i(t,\tau) w\left(\frac{\tau-\tau_f}{\alpha}\right) e^{-2\pi\sqrt{-1}f\tau}\,\mathrm{d}\tau \\ w(\tau) = H(1-|\tau|)H(|\tau|-1+r)\sin^2\left(\dfrac{|\tau|-1}{2r}\pi\right) \\ \qquad\qquad + H(1-r-|\tau|) \\ \tau_f = \dfrac{0.5}{f_1-f_0}(f-f_0), \end{cases} \tag{1}$$

where H is a Heaviside step function; $\alpha = 0.01$ s; $r = 0.1$ s; τ_f is the time when the signal was designed to have power, in the frequency range 2000 Hz $\leq$ f $\leq$ 49000 Hz; and f_0 and f_1 represent the sweep signal's starting and ending frequencies, i.e., $f_0 = 1000$ Hz and $f_1 = 50000$ Hz. It should be noted that the spectra $U_i(t,f)$ may include effects of reflected and/or refracted waves from the free surface of the sand, the container's walls and the interfaces of bentonite layer; in the following, we investigated the stability of the transmitted waves including these phases.

Third, we extracted only the propagation characteristics of the medium from the recorded waves to examine their stability. The recorded waves $u_i(t,\tau)$ were represented by a convolution of the characteristics of a source, propagation of waves through a medium, and a measurement instrument. The source characteristics are independent of channel label i, since the source was common to all channels. In addition, the source characteristics are almost independent of the measurement time t and almost identical to each other for both dry and nearly saturated conditions, as described in "Stability of the transmitted waves in our system" and "Monitoring capability for water content change in our system" section. The characteristics of the measurement instrument are independent of the measurement time. We removed the source and the instrument terms and extracted only the propagation characteristics as follows. In the frequency domain, $U_i(t,f)$ can be represented by a multiplication:

$$U_i(t,f) = S(f)G_i(t,f)I_i(f) \tag{2}$$

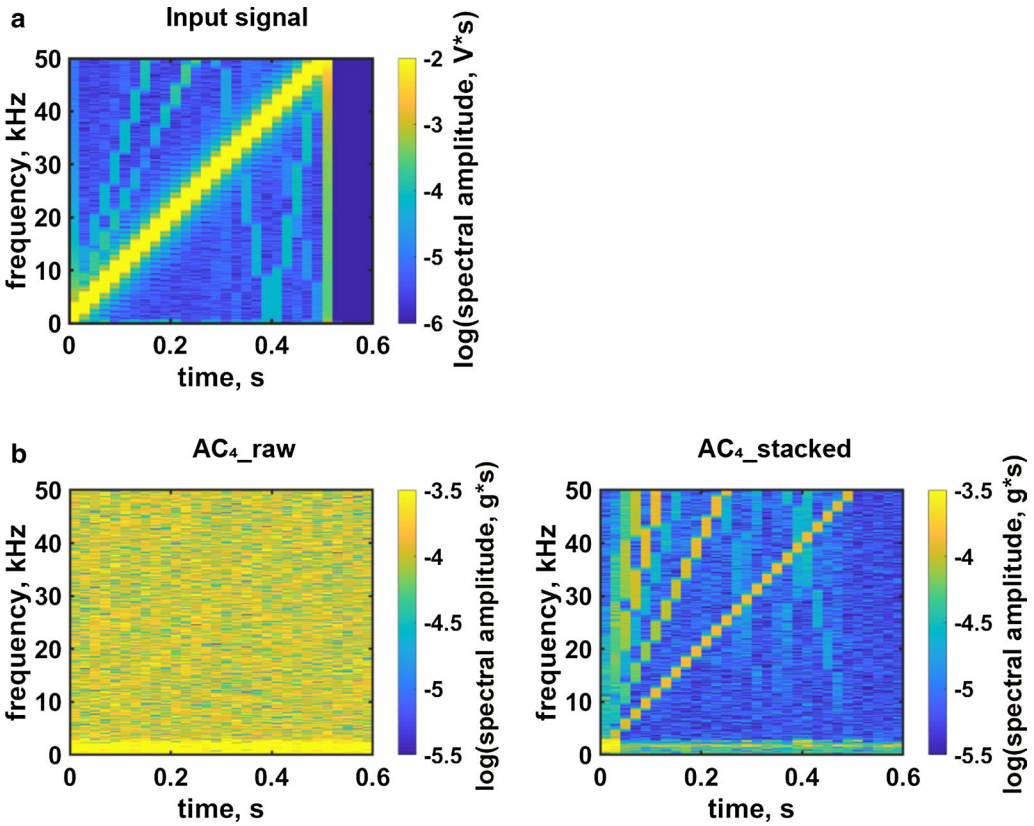

Fig. 4 **a** Typical spectrograms of the stacked waveform for the input signal. **b** Typical spectrograms of the raw waveform (left) and the stacked waveform (right) for the most distant receiver, AC_4, under dry conditions

where $S(f)$, $G_i(t,f)$, and $I_i(f)$ represent the Fourier transform for the characteristics for the source, propagation, and measurement instrument, respectively. We can remove the source effects by normalizing $U_i(t,f)$ by $U_{\mathrm{ref}}(t,f)$:

$$\frac{U_i(t,f)}{U_{\mathrm{ref}}(t,f)} = \frac{S(t,f)G_i(t,f)I_i(f)}{S(t,f)G_{\mathrm{ref}}(t,f)I_{\mathrm{ref}}(f)} = \frac{G_i(t,f)I_i(f)}{G_{\mathrm{ref}}(t,f)I_{\mathrm{ref}}(f)}. \tag{3}$$

Furthermore, we can extract only the propagation characteristics:

$$\begin{aligned}\frac{U_i(t,f)}{U_{\mathrm{ref}}(t,f)} \Big/ \frac{\overline{U_i(f)}}{\overline{U_{\mathrm{ref}}(f)}} &= \frac{G_i(t,f)I_i(f)}{G_{\mathrm{ref}}(t,f)I_{\mathrm{ref}}(f)} \Big/ \frac{\overline{G_i(f)}I_i(f)}{\overline{G_{\mathrm{ref}}(f)}I_{\mathrm{ref}}(f)} \\ &= \frac{G_i(t,f)}{\overline{G_i(f)}} \Big/ \frac{G_{\mathrm{ref}}(t,f)}{\overline{G_{\mathrm{ref}}(f)}},\end{aligned} \tag{4}$$

where the overline denotes the average over 24 h.

Finally, we separated the calculated spectrum in Eq. (4), i.e., $\frac{U_i(t,f)}{U_{\mathrm{ref}}(t,f)} \Big/ \frac{\overline{U_i(f)}}{\overline{U_{\mathrm{ref}}(f)}}$, into amplitude and phase components. We defined the normalized spectral amplitude propagator and normalized phase propagator as follows:

$$\begin{cases} A_i(t,f) = \left| \frac{U_i(t,f)}{U_{\mathrm{ref}}(t,f)} \Big/ \frac{\overline{U_i(f)}}{\overline{U_{\mathrm{ref}}(f)}} \right| \\ \Delta\phi_i(t,f) = \arg\left(\frac{\mathrm{U_i(t,f)}}{\mathrm{U_{ref}(t,f)}} \Big/ \frac{\overline{\mathrm{U_i(f)}}}{\overline{\mathrm{U_{ref}(f)}}} \right) + 2\mathrm{m_i(t,f)}\pi, \end{cases} \tag{5}$$

where $-\pi \le \arg\left(\frac{\mathrm{U_i(t,f)}}{\mathrm{U_{ref}(t,f)}} \Big/ \frac{\overline{\mathrm{U_i(f)}}}{\overline{\mathrm{U_{ref}(f)}}} \right) < \pi$ and $m_i(t,f)$ is an integer. Note that $A_i(t,f)$ and $\Delta\phi_i(t,f)$ were smoothed in the frequency domain by calculating moving means with a 2 kHz wide window.

Results and discussion

Improvement of S/N ratios of the stacked waveforms

We examined whether the stacking process improved the S/N ratios. Figure 4b shows typical spectrograms of the raw waveform (left) and the stacked waveform (right) for the most distant accelerometer, AC_4, under the dry condition. With the stacking, the amplitude of the fundamental tones was maintained, whereas that of the background noise was reduced. The resulting S/N ratios exceeded ten almost everywhere under both dry and nearly saturated

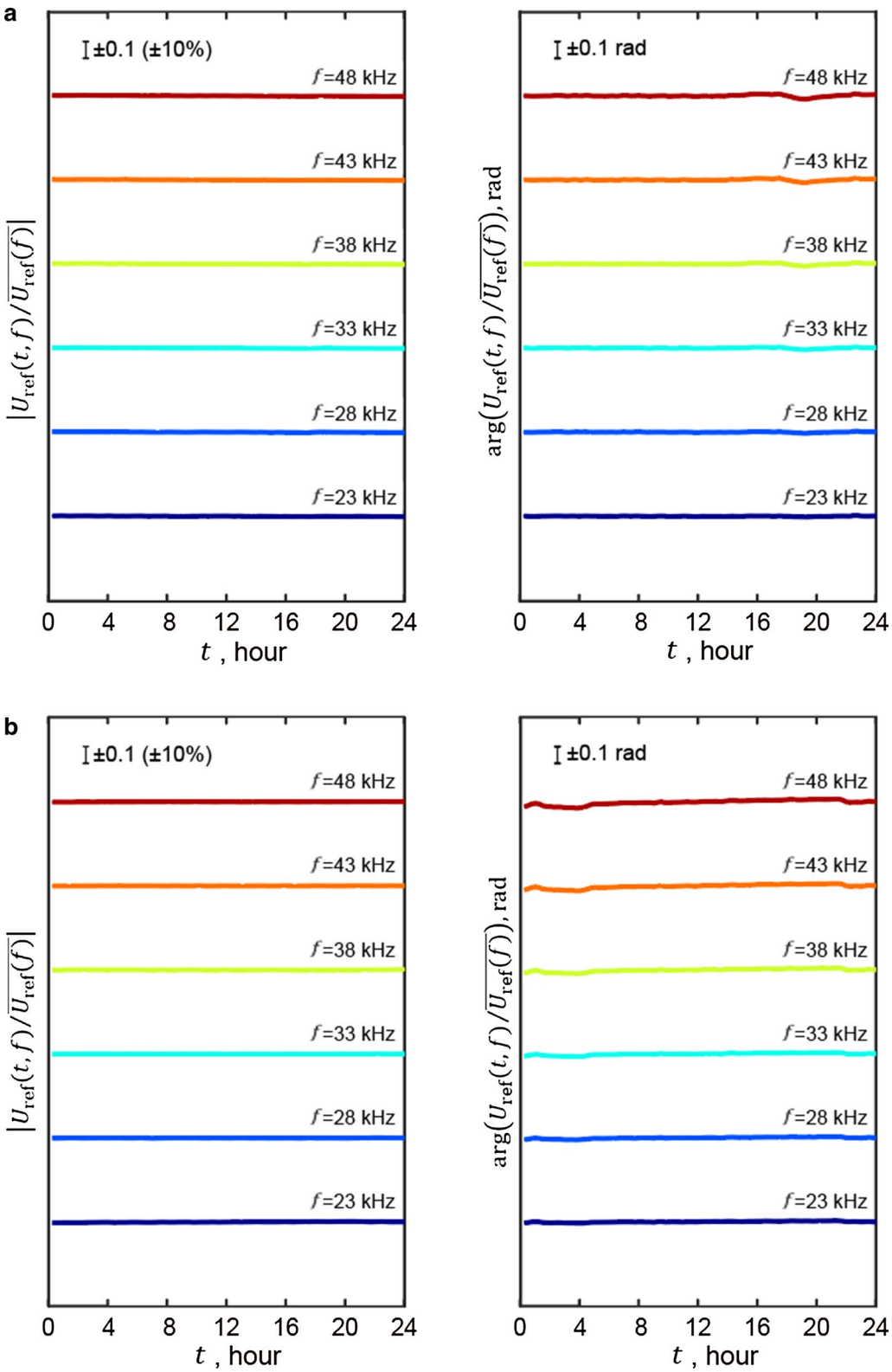

Fig. 5 Time histories of normalized amplitude and normalized phase for AC_{ref} under **a** dry and **b** nearly saturated conditions

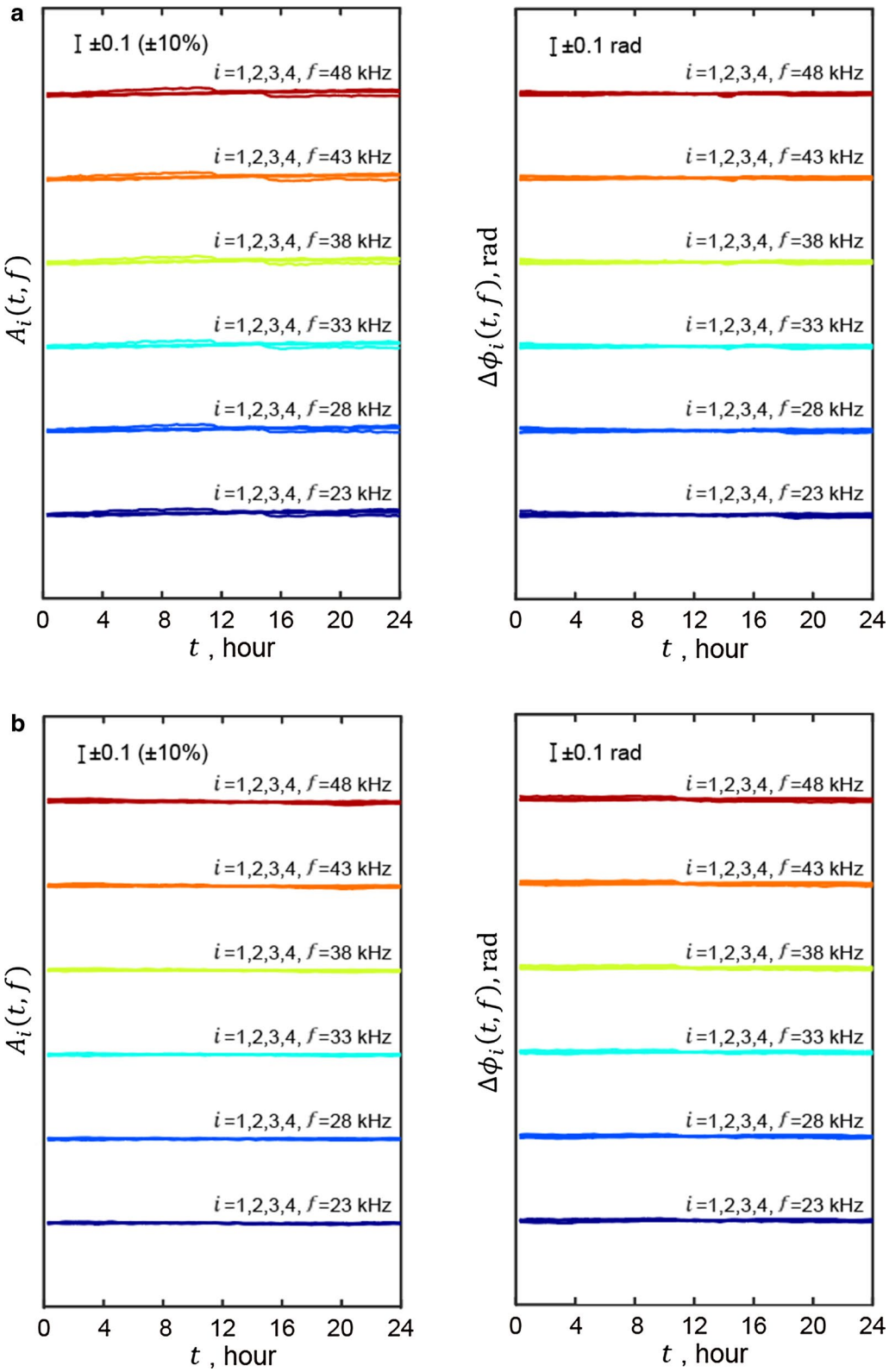

Fig. 6 Time histories of the normalized amplitude propagator and normalized phase propagator under **a** dry and **b** nearly saturated conditions

conditions. If there were non-negligible phase variations in the raw waveforms, they would be incoherent and cancel each other out when they were stacked, which would fail to improve the S/N ratio. Thus, the improvement in S/N ratios suggested that phase variations within 15 min for the raw waveforms were negligible.

Stability of the transmitted waves in our system

We examined the stability of the transmitted waves over 24 h under dry and nearly saturated conditions to estimate the capability of monitoring the water content change. First, we checked the stability of the shaker's output. The amplitude and phase for AC_{ref}, i.e., $\left|U_{\mathrm{ref}}(t,f)/\overline{U_{\mathrm{ref}}(f)}\right|$ and $\arg\left(\mathrm{U_{ref}(t,f)/\overline{U_{ref}(f)}}\right)$, were stable between 23 and 49 kHz, and their standard deviations were within $\pm 0.8\%$ and ± 0.03 rad, respectively, under both conditions (Fig. 5). Note that $\left|U_{\mathrm{ref}}(t,f)/\overline{U_{\mathrm{ref}}(f)}\right|$ and $\arg\left(\mathrm{U_{ref}(t,f)/\overline{U_{ref}(f)}}\right)$ were smoothed in the frequency domain by calculating moving means with a 2 kHz wide window. Their standard deviations below 23 kHz were larger, so we limited the frequency band between 23 and 49 kHz thereafter.

Next, we investigated the stability of the transmitted waves. Figure 6 shows time histories of the normalized amplitude propagator, $A_i(t,f)$, and the normalized phase propagator, $\Delta\phi_i(t,f)$, every 5 kHz. Beforehand, we considered the ambiguity of the cycle of phase change, i.e., $m_i(t,f)$ in Eq. (5). We confirmed that the phase variations within 15 min were negligible, as discussed in "Improvement of S/N ratios of the stacked waveforms" section. The small phase variations in the stacked waveforms (Fig. 6) mean that $m_i(t,f)$ should be constant. Considering that the expected value of $\Delta\phi_i(t,f)$ is zero, $m_i(t,f)=0$. The standard deviations of $A_i(t,f)$ and $\Delta\phi_i(t,f)$ were within $\pm 3\%$ and ± 0.03 rad (equivalent to the changes in travel time from 0.2 μs at 49 kHz to 0.4 μs at 23 kHz), respectively.

Monitoring capability for water content change in our system

We estimated the capability of monitoring the water content change in our system. The maximum change in the equivalent travel time was 0.4 μs. In other words, the fluctuation in the slowness (i.e., inverse velocity) was 4 μs/m, which is the resolution of the change in slowness in our system (refer to Additional file 1 for an explanation of the use of slowness instead of velocity). By visually estimating the travel times of the stacked waveforms, we estimated that the velocities under dry and nearly saturated conditions were 65 m/s and 120 m/s, respectively (Fig. 7). This lower velocity under the nearly saturated condition than that predicted by Gassmann's fluid substitution equations in consolidated and unconsolidated material (Berryman 1999) may be because of the air in the tap water and/or due to the imperfect imbibition method. The expected difference in slowness between the two conditions was 7 ms/m. This difference was one-thousand-fold greater

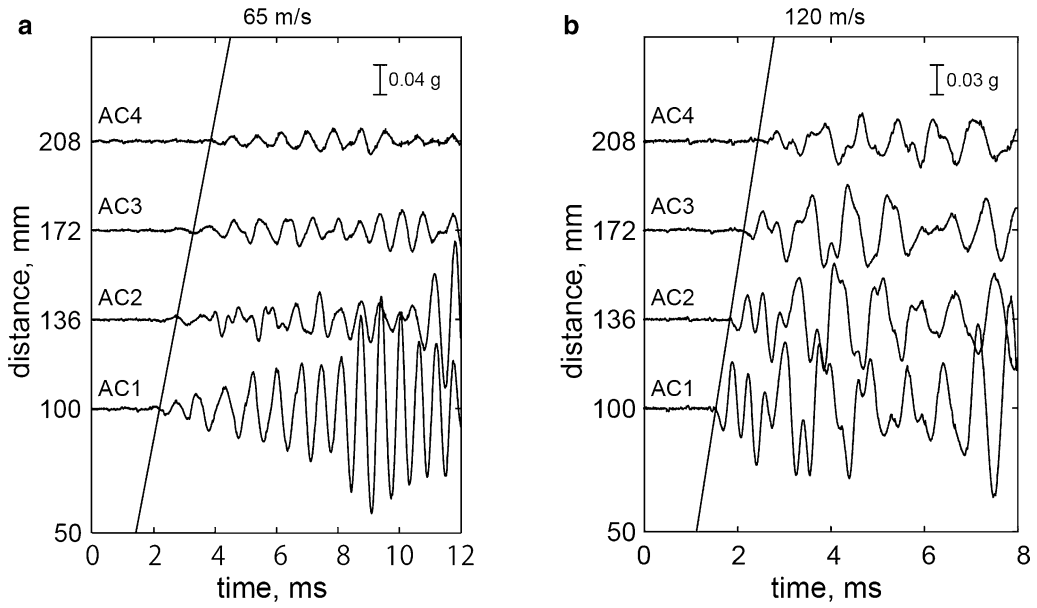

Fig. 7 The record sections of stacked waveforms at the initial measurements under **a** dry and **b** nearly saturated conditions. A fourth-order Butterworth band-pass filter from 0.1 to 100 kHz was applied to the waveforms. Oblique lines denote arrival times

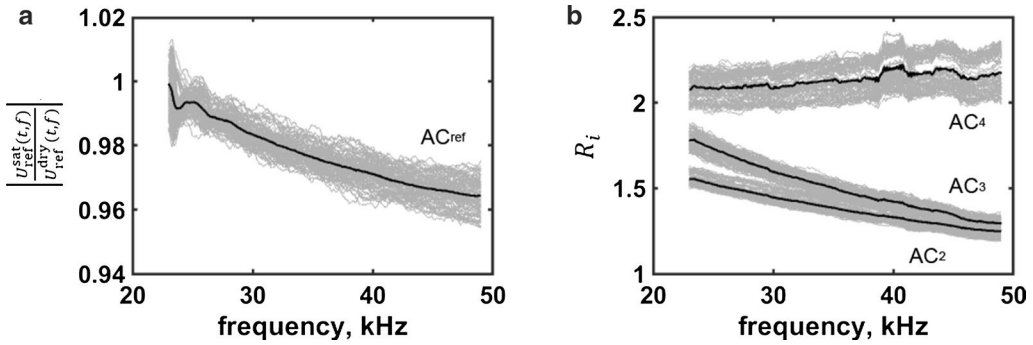

Fig. 8 Spectral amplitude ratios between dry and nearly saturated conditions. See "Monitoring capability for water content change in our system" section for definitions of **a** $\left|\frac{U_{\mathrm{ref}}^{\mathrm{sat}}(t,f)}{U_{\mathrm{ref}}^{\mathrm{dry}}(t,f)}\right|$ and **b** $R_i(t,f)$. Gray and black lines represent the amplitude ratios for each stacked waveform and their averages, respectively

than the resolution of the change in slowness in our system. Therefore, we may be able to monitor the water content change via changes in slowness.

We also compared the amplitudes between dry and nearly saturated conditions. When the amplitude differences between the two conditions for the receivers were larger than those for the shaker, then the water content can also be monitored from the amplitude. Figure 8a shows the averages and all the data over 24 h of the amplitude ratios between both conditions for $\mathrm{AC}_{\mathrm{ref}}$, $\left|\frac{U_{\mathrm{ref}}^{\mathrm{sat}}(t,f)}{U_{\mathrm{ref}}^{\mathrm{dry}}(t,f)}\right|$. The suffixes "dry" and "sat" denote values under dry and nearly saturated conditions, respectively. Note that $\left|\frac{U_{\mathrm{ref}}^{\mathrm{sat}}(t,f)}{U_{\mathrm{ref}}^{\mathrm{dry}}(t,f)}\right|$ was smoothed in the frequency domain by calculating the moving means with a 2 kHz wide window. The standard deviations of the ratios for 24 h were within 1%, and the ratios ranged from 0.95 to 1 for all the frequencies.

Under nearly saturated conditions, the bentonite layer (BL) may reflect the waves unexpectedly. Therefore, we needed to compare the amplitude between the two conditions after removing the effects of the reflection boundary. Then, we normalized the spectra of stacked waveforms for each channel by those for AC_1 installed in the permeable part (PP). We calculated the amplitude ratios between the two conditions and extracted only the propagation characteristics:

$$\begin{aligned} R_i(t,f) &= \left|\frac{U_i^{\mathrm{sat}}(t,f)}{U_1^{\mathrm{sat}}(t,f)}\right| \Big/ \left|\frac{U_i^{\mathrm{dry}}(t,f)}{U_1^{\mathrm{dry}}(t,f)}\right| \\ &= \left|\frac{G_i^{\mathrm{sat}}(t,f)I_i(f)}{G_1^{\mathrm{sat}}(t,f)I_1(f)}\right| \Big/ \left|\frac{G_i^{\mathrm{dry}}(t,f)I_i(f)}{G_1^{\mathrm{dry}}(t,f)I_1(f)}\right| \\ &= \left|\frac{G_i^{\mathrm{sat}}(t,f)}{G_1^{\mathrm{sat}}(t,f)}\right| \Big/ \left|\frac{G_i^{\mathrm{dry}}(t,f)}{G_1^{\mathrm{dry}}(t,f)}\right|, \end{aligned} \tag{6}$$

where we assume that I_i/I_1 is independent of these conditions, and the source terms were removed as in Eq. (3). $R_i(t,f)$ represents the amplitude ratios between both dry and nearly saturated conditions for $G_i(t,f)$ normalized by $G_1(t,f)$. Figure 8b shows the averages and all the data over 24 h of the ratios $R_i(t,f)$ for each receiver. Note that $R_i(t,f)$ was smoothed in the frequency domain by calculating moving means with a 2 kHz wide window. The standard deviations over 24 h were within 11%, and $R_i(t,f)$ was larger than 1.2 for all the frequencies. Therefore, the magnitude of $R_i(t,f)$, the difference in the propagation characteristics between the dry and nearly saturated conditions, was about double the value of its fluctuations. Also, the amplitude change may enable us to monitor the water content change. The frequency dependence of $R_4(t,f)$ differs from $R_2(t,f)$ and $R_3(t,f)$, which might be explained by each behavior of $\left|\frac{U_i^{\mathrm{dry}}(t,f)}{U_1^{\mathrm{dry}}(t,f)}\right|$ or $\left|\frac{U_i^{\mathrm{sat}}(t,f)}{U_1^{\mathrm{sat}}(t,f)}\right|$ (refer to Additional file 2). $\left|\frac{U_i^{\mathrm{dry}}(t,f)}{U_1^{\mathrm{dry}}(t,f)}\right|$ or $\left|\frac{U_i^{\mathrm{sat}}(t,f)}{U_1^{\mathrm{sat}}(t,f)}\right|$ seems to include two propagation effects; one is a negatively frequency-dependent effect by a normal type of attenuation and the other is an unknown positively frequency-dependent effect. The negative effect tends to be dominant at far field. For the unknown positive effect, it is necessary to investigate whether the effect is real or

artificial due to the configuration of our experiment, for example.

Applicability of our system

In the following, we discuss the applicability of our system in fields, such as geohazard risk reduction and geophysics. First, our system can be used to help with monitoring in field observations of slopes. We succeeded in developing a measurement system that allows us to observe the transmitted waves with a broader and higher frequency band, i.e., we expanded the range of the wavelength λ relative to the sensor intervals x. Although it is impossible to immediately compare laboratory experimental results and field observations as described in "Introduction" section, expanding the range of λ can help fill a gap in understanding in velocity dispersion and attenuation of transmitted waves. If the transmitted waves change in amplitude and velocity at frequencies depending on the characteristic sizes of the fluid distribution within slopes, then broadband monitoring like our system could help us understand spatiotemporal variations in the characteristic sizes of the fluid distribution in detail.

Second, our system may help in the theoretical understanding of wave attenuation and velocity dispersion due to pore fluids in unconsolidated and porous media. In rock physics, theoretical and experimental works have revealed that the amount of pore fluids in porous rocks affects velocity dispersion and attenuation of transmitted elastic waves as reviewed by Müller et al. (2010). On the other hand, for unconsolidated and porous materials, George et al. (2009) observed that the velocity reached its maximum at full saturation and quickly decreased when air was introduced into the samples, then it slightly recovered at a lower water saturation level. They mentioned that the trend of the change in velocity in their narrow frequency range was consistent with the theoretical model of Lo et al. (2007). Barrière et al. (2012) observed that the velocity gradually decreased during the imbibition and increased during the drainage. The attenuation strengthened around the middle saturation degree during the imbibition and slightly weakened during the drainage. They checked that the experimental results in their narrow frequency range were consistent with a model established for partially saturated unconsolidated and porous materials based on Biot's theory, a framework for velocity dispersion and attenuation in fully saturated porous rocks. Our system with waves in a broader frequency range may help extend their attempt to a wide frequency range in the future. For example, it is possible to perform post-processing for the responses to sweep source signals with an analogy of processing for vibroseis to estimate velocity dispersion and attenuation (e.g., Sun et al. 2009).

Conclusion

We developed a measurement system that enables us to investigate relationships between elastic wave propagation transmitted through sand and water saturation. We installed a shaker to repeatedly emit arbitrary and identical signals with a broader and higher frequency band and proposed a technique that prevents any changes in the coupling between the shaker and the sand due to changes in the degree of water saturation. We measured the transmitted waves through the sand over 24 h under two static conditions: dry and nearly saturated. Then, we estimated the capability of monitoring the water content change in our system by comparing the fluctuations in slowness and amplitude with the differences in slowness and amplitude between the two conditions. The differences were more significant than the fluctuations, which suggested that we succeeded in transmitting waves with a broader and higher frequency band, and our system can monitor the water content change in sand via the change in spectral amplitude and phase slowness. The monitoring of velocity dispersion and attenuation in a broader frequency range under various water content levels may help integrate experimental/field results and theoretical studies in a wide frequency range.

Supplementary Information

The online version contains supplementary material available at https://doi.org/10.1186/s40623-020-01346-4.

Additional file 1. Reason for using slowness instead of velocity.

Additional file 2. Amplitude ratios for each accelerometer under dry and nearly saturated conditions.

Abbreviations

PP: Permeable part; IP: Impermeable part; BL: Bentonite layer; FG: Function generator.

Acknowledgements

We thank two anonymous reviewers and the editor for providing comments that are helpful to improve the manuscript.

Authors' contributions

MN developed the measurement system, analyzed all the recorded data, discussed the results and wrote the manuscript. HK and SH contributed to establishing the system. HK, SH, and ID participated in the discussion. All authors read and approved the final manuscript.

Funding

This research was supported by JSPS KAKENHI (JP15H02996 and 26750135).

Availability of data and materials
The data are available from the corresponding author upon reasonable request.

Ethics approval and consent to participate
Not applicable.

Consent for publication
Not applicable.

Competing interests
The authors declare that they have no competing interests.

Author details
[1] Graduate School of Science and Engineering, Ritsumeikan University, 1-1-1, Noji-Higashi, Kusatsu, Shiga 525-8577, Japan. [2] College of Science and Engineering, Ritsumeikan University, 1-1-1, Noji-Higashi, Kusatsu, Shiga 525-8577, Japan. [3] Disaster Prevention Research Institute, Kyoto University, Gokasho, Uji, Kyoto 611-0011, Japan.

Received: 10 August 2020 Accepted: 24 December 2020
Published online: 22 January 2021

References

Barrière J, Bordes C, Brito D, Senechal P, Perroud H (2012) Laboratory monitoring of *P* waves in partially saturated sand. Geophys J Int 191:1152–1170. https://doi.org/10.1111/j.1365-246X.2012.05691.x

Berryman JG (1999) Origin of Gassmann's equations. Geophysics 64:1627–1629. https://doi.org/10.1190/1.1444667

Brückl E, Brunner FK, Land E, Mertl S, Müller M, Stary U (2013) The Gradenbach Observatory—monitoring deep-seated gravitational slope deformation by geodetic, hydrological, and seismological methods. Landslides 10:815–829. https://doi.org/10.1007/s10346-013-0417-1

Chen Y, Irfan M, Uchimura T, Cheng G, Nie W (2018a) Elastic wave velocity monitoring as an emerging technique for rainfall-induced landslide prediction. Landslides 15:1155–1172. https://doi.org/10.1007/s10346-017-0943-3

Chen Y, Irfan M, Uchimura T, Ke Z (2018b) Feasibility of using elastic wave velocity monitoring for early warning of rainfall-induced slope failure. Sensors 18:997. https://doi.org/10.3390/s18040997

Chen Y, Irfan M, Uchimura T, Wu Y, Yu F (2019) Development of elastic wave velocity threshold for rainfall-induced landslide prediction and early warning. Landslides 16:955–968. https://doi.org/10.1007/s10346-019-01138-2

Emerson M, Foray P (2006) Laboratory P-wave measurements in dry and saturated sand. Acta Geotech 1:167–177. https://doi.org/10.1007/s11440-006-0015-7

García-Delgado H, Machuca S, Medina E (2019) Dynamic and geomorphic characterizations of the Mocoa debris flow (March 31, 2017, Putumayo Department, southern Colombia). Landslides 16:597–609. https://doi.org/10.1007/s10346-018-01121-3

George LA, Dewoolkar MM, Znidarcic D (2009) Simultaneous laboratory measurement of acoustic and hydraulic properties of unsaturated soils. Vadoes Zone J 8:633–642. https://doi.org/10.2136/vzj2008.0139

Lo WC, Yeh CL, Tsai CT (2007) Effect of soil texture on the propagation and attenuation of acoustic wave at unsaturated conditions. J Hydrol 338:273–283. https://doi.org/10.1016/j.jhydrol.2007.02.034

Lorenzo JM, Smolkin DE, White C, Chollett SR, Sun T (2013) Benchmark hydrogeophysical data from a physical seismic model. Comput Geosci 50:44–51. https://doi.org/10.1016/j.cageo.2012.07.034

Mainsant G, Larose E, Brönnimann C, Jongmans D, Michoud C, Jaboyedoff M (2012) Ambient seismic noise monitoring of a clay landslide: toward failure prediction. J Geophys Res 117:F01030. https://doi.org/10.1029/2011JF002159

Müller TM, Gurevich B, Lebedev M (2010) Seismic wave attenuation and dispersion resulting from wave-induced flow in porous rocks—a review. Geophysics 75(26):A147–A164. https://doi.org/10.1190/1.3463417

Pride SR (2005) Relationships between seismic and hydrological properties. Hydrogeophysics 50:253–290. https://doi.org/10.1007/1-4020-3102-5_9

Sun LF, Milkereit B, Schmitt DR (2009) Measuring velocity dispersion and attenuation in the exploration seismic frequency band. Geophysics 74:113–122. https://doi.org/10.1190/1.3068426

Taylor OD, Cunningham AL, Walker RE, Mckenna MH, Martin KE, Kinnebrew PG (2019) The behavior of near-surface soils through ultrasonic near-surface inundation testing. Near surface Geophys 17:331–344. https://doi.org/10.1002/nsg.12045

Wang F, Wu YH, Yang H, Tanida Y, Kamei A (2015) Geoenviron Disast 2:17. https://doi.org/10.1186/s40677-015-0025-6

Zhou JW, Cui P, Hao MH (2015) Comprehensive analyses of the initiation and entrainment processes of the 2000 Yigong catastrophic landslide in Tibet, China. Landslides 13:39–54. https://doi.org/10.1007/s10346-014-0553-2

Publisher's Note